Chiral metamaterials: from optical activity and negative refractive index to asymmetric transmission

REVIEW ARTICLE

Chiral metamaterials: from optical activity and negative refractive index to asymmetric transmission

Zhaofeng Li[1,2], Mehmet Mutlu[1,2] and Ekmel Ozbay[1,2,3]

[1] Nanotechnology Research Center, Bilkent University, Bilkent, 06800 Ankara, Turkey
[2] Department of Physics, Bilkent University, Bilkent, 06800 Ankara, Turkey
[3] Department of Electrical and Electronic Engineering, Bilkent University, Bilkent, 06800 Ankara, Turkey

E-mail: zhaofengli@bilkent.edu.tr and ozbay@bilkent.edu.tr

Abstract

We summarize the progress in the development and application of chiral metamaterials. After a brief review of the salient features of chiral metamaterials, such as giant optical activity, circular dichroism, and negative refractive index, the common method for the retrieval of effective parameters for chiral metamaterials is surveyed. Then, we introduce some typical chiral structures, e.g., chiral metamaterial consisting of split ring resonators, complementary chiral metamaterial, and composite chiral metamaterial, on the basis of the studies of the authors' group. The coupling effect during the construction of bulk chiral metamaterials is mentioned and discussed. We introduce the application of bianisotropic chiral structures in the field of asymmetric transmission. Finally, we mention a few directions for future research on chiral metamaterials.

(Some figures may appear in colour only in the online journal)

1. Introduction

Metamaterials are artificially structured media that are engineered to possess electromagnetic properties that do not exist in natural materials, and one typical instance is the well-known negative refraction. The first negative index metamaterial (NIM) [1] consists of two ingredients: one is the continuous metallic wires that provide negative permittivity [2], and the other is the split ring resonators (SRRs) that provide negative permeability [3]. The simultaneous negative permittivity and permeability can result in the negative refractive index. Subsequently, most of the metamaterials that are designed for the negative refractive index were based on this principle [4–6]. Although negative permeability (using split ring resonators, for instance) can be easily obtained in the microwave frequency range, that is not the case in the optical frequency range [7, 8]. Meanwhile, an alternative route to realizing negative refraction by utilizing chirality was proposed theoretically by several independent groups, i.e., those of Pendry [9], Tretyakov [10, 11], and Monzon [12]. It was also demonstrated theoretically that a chiral medium slab can be used as a perfect lens [9–13]. Among the reports, Pendry suggested a three-dimensional (3D) helix structure (a chiral variant of the Swiss roll structure) for realizing a chiral metamaterial (CM) with negative refraction [9]. Tretyakov *et al* theoretically studied

the possibilities for obtaining a negative refraction in chiral composites consisting of chiral and dipole particles [11]. It was shown theoretically that a negative refractive index can be obtained in a metamaterial made of metallic spheres arranged in a 3D lattice of helicoidal symmetry [14]. It was also shown that periodic arrangements of chiral scatterers can provide 3D and isotropic negative refractive index media [15]. In fact, Bose once studied the rotation of the plane of polarization of electromagnetic waves by a twisted structure in 1898 [16]. Lindman was also a pioneer in the microwave study of a chiral artificial medium [17]. Recently, Zhang *et al* experimentally demonstrated a 3D chiral metamaterial with a negative refractive index that works in the THz regime [18]. Wang *et al* also demonstrated with experiments in the microwave regime that 3D chiral metamaterials give not only a negative refractive index, but also giant optical activity and circular dichroism [19, 20]. However, these above mentioned 3D chiral metamaterials are usually difficult to fabricate. Meanwhile, it was reported that planar chiral structures can also exhibit optical activity [21–24]. It should be noted here that a planar chiral structure is different from a true chiral structure (or 3D chiral structure). Arnaut and Davis first introduced planar chiral structures into electromagnetic research [25, 26]. A structure is defined as chiral if it lacks any planes of mirror symmetry, while a planar object is considered a planar chiral structure if it cannot be superimposed on its in-plane mirror image (reflected by a mirror perpendicular to the plane of the structure) unless it is lifted from the plane. In practice, a planar chiral structure still possesses mirror symmetry for the mirror in the plane. At normal incidence, a structure with a symmetric configuration in the propagation direction exhibits no optical activity [27]. Nevertheless, this situation can be changed by adding a substrate to the structure that breaks the symmetry in the propagation direction, and optical activity can thus be obtained [22–24]. However, chirality is usually quite small in these structures. Later, Rogacheva *et al* went a further step, and they demonstrated giant optical activity in a bilayered chiral structure [28]. The two layers of planar metal rosette patterns are located in parallel planes twisting with respect to each other, and they are not directly connected as in the 3D chiral unit cells [18–20] but can couple to each other electromagnetically. The optical activity is so strong that the whole structure shows a signature of a negative refractive index. Following this pioneering work, several different bilayered chiral structures working in the regimes from microwave to infrared were proposed, e.g., bilayered rosette structure [29, 30], bilayered cross-wire structure [31, 32], metallic cut wire pairs [33], conjugated gammadion structure [34], four-'U'-shape structure [35–37], complementary chiral structure [38], etc. Moreover, chiral metamaterials consisting of more than two layers of planar structures were also investigated [29, 39]. It was shown that to construct a bulk chiral metamaterial, the effect of coupling between neighboring unit cells should be taken into account. Due to the existence of the coupling effect, the bulk chiral metamaterial and one unit cell of the chiral metamaterial have different properties [39]. When a chiral metamaterial is working at a band of negative refractive index, there is a

figure of merit (FOM) parameter for evaluating its degree of loss [40]. FOM is defined as the absolute value of the ratio between the real and imaginary parts of the refractive index ($|\mathrm{Re}(n)/\mathrm{Im}(n)|$). Over a length corresponding to one medium wavelength λ, the wave amplitude decays to $\exp(-2\pi/\mathrm{FOM})$. In order to achieve a high FOM value, a composite chiral metamaterial was proposed recently [41]. Moreover, tunable chiral metamaterials were also reported [42].

The retrieval of the effective refractive index on the basis of the transmission and reflection parameters is a convenient and useful tool for characterizing a designed metamaterial [43–47]. Along with the progress in the study of chiral metamaterials, a negative refractive index was also obtained by several retrieval methods [18, 29, 48, 49]. Zhao *et al* summarized these retrieval methods with several concise formulas that can be used effectively in the studies of chiral metamaterials [50].

Nonreciprocal transmission plays a fundamental role in information processing, and the electrical diode is a typical example that shows a nonreciprocal response in electric circuits, which stimulates considerable effort devoted to the study of the nonreciprocal propagation of light. There are two conventional methods for achieving nonreciprocity in optics. One method is to use a magneto-optical medium that breaks the time-reversal symmetry by introducing a set of antisymmetric off-diagonal dielectric tensor elements [51]. The other method is to use a nonlinear medium [52, 53]. Nonetheless, it has been demonstrated that nonreciprocal light propagation can be realized by the breaking of parity–time symmetry with complex optical potentials [54]. Meanwhile, there were attempts to achieve asymmetric but still reciprocal transmission by using conventionally isotropic, linear, and lossy or lossless materials. For instance, the asymmetric transmission of linearly polarized waves can be realized by using diffractive nonsymmetrical volumetric gratings based on photonic crystals [55], and using nonsymmetrical metallic gratings supporting surface plasmons [56]. In a diffraction scenario, asymmetric transmission was demonstrated by using a planar chiral array [57]. The asymmetric transmission of circularly polarized waves has been demonstrated at normal incidence by using a planar chiral structure consisting of a single layer of meta-atoms [58–60]. A thin structure composed of 3D meta-atoms without any rotational symmetry was proposed to achieve asymmetric transmission for an arbitrary (including linear and circular) polarization of the incident electromagnetic wave [61]. It has been demonstrated that asymmetric transmission can also be achieved with chiral metamaterials after slight changes to the structure [62, 63].

The remainder of this review is arranged as follows. In section 2 we give a brief overview of the physical properties of a typical chiral medium, and revisit the retrieval process for chiral metamaterials. In section 3 we introduce several typical chiral metamaterials with negative refractive indices and their characteristics. In section 4 we mention the construction of bulk chiral metamaterials. In section 5 we introduce two cases of asymmetric transmissions based on deformed chiral structures. Section 6 summarizes the review and gives some perspectives for future studies.

2. The physical properties of chiral metamaterials and retrieval of the effective parameters

2.1. The physical properties of a chiral medium

In terms of the electromagnetic response, chiral material is characterized by a cross-coupling between electric and magnetic fields along the same direction. The electromagnetic wave propagation in such a chiral structure obeys the following constitutive relations [64]:

$$\begin{pmatrix} D \\ B \end{pmatrix} = \begin{pmatrix} \varepsilon_0 \varepsilon_r & -i\kappa/c \\ i\kappa/c & \mu_0 \mu_r \end{pmatrix} \begin{pmatrix} E \\ H \end{pmatrix} \tag{1}$$

where ε_0 and μ_0 are the permittivity and permeability of vacuum. ε_r and μ_r are the relative permittivity and permeability of the chiral medium. c is the speed of light in vacuum. κ is the chirality that measures the effect of cross-coupling between electric and magnetic fields. Due to the existence of κ, the degeneracy of the two circularly polarized waves is broken; i.e., the refractive index is increased for one circular polarization and reduced for the other. Assuming a time dependence of $e^{-i\omega t}$, the right circularly polarized (RCP, $+$) wave and left circularly polarized (LCP, $-$) wave are defined as $E_\pm = \frac{1}{2} E_0 (\hat{x} \mp i\hat{y})$ [65]. The refractive index for RCP and LCP waves is obtained as follows [64]:

$$n_\pm = \sqrt{\varepsilon_r \mu_r} \pm \kappa = n_0 \pm \kappa. \tag{2}$$

At the same time, RCP and LCP waves have the same impedance of $Z = Z_0 \sqrt{\mu_r/\varepsilon_r}$, where Z_0 is the impedance of the vacuum. Given the fact that the chirality κ is strong enough, negative refraction may occur for one circularly polarized wave even when both ε_r and μ_r are positive, while for the other circular polarization the refractive index remains positive. This constitutes Pendry's earlier proposal of an alternative route to realizing a negative refractive index [9].

A chiral medium has two important properties. One is called optical activity, which characterizes the rotation of the polarization plane of linearly polarized light as it passes through a chiral medium. Mathematically, it is defined as the polarization azimuth rotation angle of elliptically polarized light:

$$\theta = [\arg(T_+) - \arg(T_-)]/2 \tag{3}$$

where T_+ and T_- are the transmission coefficients for RCP and LCP waves. The other property is the ellipticity angle η of the transmitted wave. It characterizes the difference between the transmissions of two polarizations:

$$\eta = \arctan[(|T_+| - |T_-|)/(|T_+| + |T_-|)]. \tag{4}$$

η also measures the circular dichroism which arises from the different absorptions for RCP and LCP waves. Artificial chiral metamaterials with large θ and small η are preferred for applications of negative refractions.
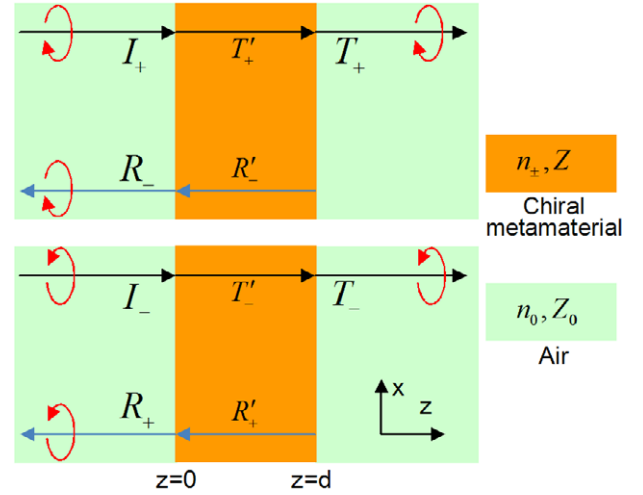
Figure 1. Schematics of the transmission and reflection coefficients of right and left circularly polarized waves for a chiral metamaterial slab.

2.2. The process of retrieval for the effective parameters

Figure 1 shows the schematics of the transmission and reflection coefficients of circularly polarized waves for a chiral metamaterial slab standing in the air.

As seen in figure 1, after applying the condition of continuity of tangential electric and magnetic fields at the two interfaces of $z = 0$ and $z = d$, the coefficients of the transmitted wave and the reflected waves have the following values when the coefficient of the incident wave is set to be unity:

$$T_\pm = \frac{4Z\, e^{in_\pm k_0 d}}{(1+Z)^2 - (1-Z)^2\, e^{i(n_+ + n_-)k_0 d}} \tag{5}$$

$$R_\pm = \frac{(1-Z)^2 (e^{i(n_+ + n_-)k_0 d} - 1)}{(1+Z)^2 - (1-Z)^2\, e^{i(n_+ + n_-)k_0 d}} \tag{6}$$

where k_0 is the wavenumber of the electromagnetic wave in the air. From equation (6), it is seen that the reflection coefficients of LCP and RCP waves are the same. Therefore, we have three unknowns (n_+, n_- and Z) that are contained in three independent equations. On the basis of the three equations, the three unknowns can be obtained as follows:
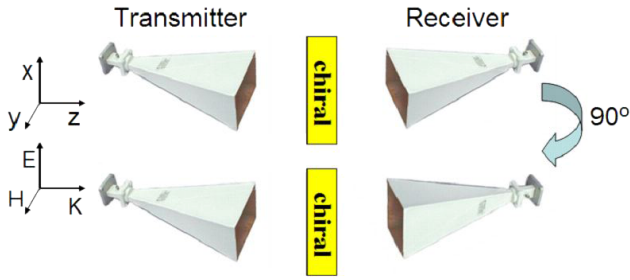
$$Z = \sqrt{\frac{(1+R)^2 - T_+ T_-}{(1-R)^2 - T_+ T_-}} \tag{7}$$

$$n_+ = \frac{i}{k_0 d} \left\{ \ln\left[\frac{1}{T_+} \left(1 - \frac{Z-1}{Z+1} R \right) \right] \pm i2m\pi \right\} \tag{8}$$

$$n_- = \frac{i}{k_0 d} \left\{ \ln\left[\frac{1}{T_-} \left(1 - \frac{Z-1}{Z+1} R \right) \right] \pm i2m\pi \right\} \tag{9}$$

where m is an integer determined by the branches. The results of equations (7)–(9) must obey the following conditions for a passive medium:

$$\mathrm{Re}(Z) \geq 0, \qquad \mathrm{Im}(n_\pm) \geq 0. \tag{10}$$

Figure 2. Schematics of the measurement method in the experiment [39]. Reproduced with permission from [39]. © 2010 OSA.

After obtaining the results for n_+, n_- and Z, other parameters can be calculated through the following relations: $n_0 = (n_+ + n_-)/2$, $\kappa = (n_+ - n_-)/2$, $\varepsilon = n_0/Z$, and $\mu = n_0 Z$.

In addition to developing the above retrieval process for a slab of chiral metamaterials, Zhao *et al* also developed the retrieval procedure for a slab of chiral metamaterial that is fabricated on a substrate [50]. However, we will not reiterate this here.

Although in practice it is usually not convenient to directly measure the transmission and reflection coefficients for circularly polarized waves, these coefficients can be calculated from the transmission and reflection coefficients of linearly polarized waves. The following formula shows the relations between the coefficients of circularly polarized waves and linearly polarized waves [31]:

$$
\begin{pmatrix} T_{++} & T_{+-} \\ T_{-+} & T_{--} \end{pmatrix}
$$
$$
= \frac{1}{2} \begin{pmatrix} t_{xx} + t_{yy} + \mathrm{i}(t_{xy} - t_{yx}) & t_{xx} - t_{yy} - \mathrm{i}(t_{xy} + t_{yx}) \\ t_{xx} - t_{yy} + \mathrm{i}(t_{xy} + t_{yx}) & t_{xx} + t_{yy} - \mathrm{i}(t_{xy} - t_{yx}) \end{pmatrix}.
$$
(11)

Figure 2 shows the schematics for the measurement of t_{xx} and t_{yx} in the experiment. If the chiral structure is of C4 rotational symmetry, then the circular polarization conversion (T_{+-}, T_{-+}) is absent, and the reflected wave of a linearly polarized incident wave remains the state of polarization. The transmission of circularly polarized waves can be converted from the linear transmission coefficients t_{xx} and t_{yx} [39]:

$$ T_\pm = t_{xx} \pm \mathrm{i} t_{yx}. \tag{12} $$

3. Several typical chiral metamaterials with negative refractive indices

Compared with the 3D chiral metamaterials, such as helix and Swiss roll structures [9, 10], the bilayered planar chiral structures are much more compatible with the planar process and easier to fabricate. Consequently, we will concentrate on the bilayered planar chiral structures in the following.

3.1. Chiral metamaterial consisting of U-shaped resonators

By stacking two mutually twisted SRRs, a magnetic dimer can be formed, and an array of these magnetic dimers can
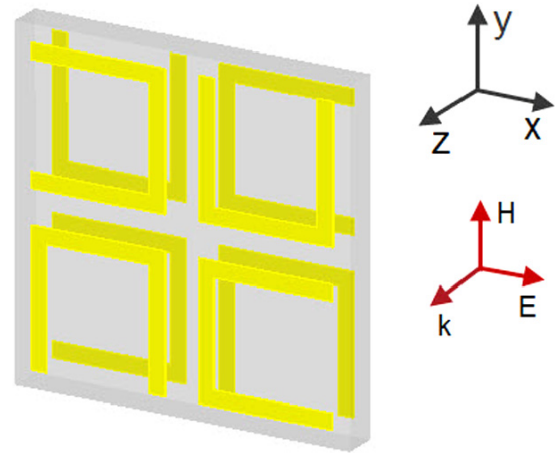
Figure 3. Schematic of a unit cell of the chiral metamaterials consisting of U-shaped split ring resonators. These copper resonators are fabricated on the opposite sides of the FR-4 board [36]. Reproduced with permission from [36]. © 2010 AIP.

possess optical activity [66, 67]. However, due to the lack of rotational symmetry, the optical activity is sensitive to the linear polarization of the incident wave. To eliminate this shortcoming, a design was proposed in which the U-shaped SRR pairs are arranged in C4 symmetry (see figure 3) [36]. The structure is periodic in the x and y directions with both of the periodic constants being 15 mm—that is, much less than the operating wavelength—and the thickness of the structure is 1.66 mm. The waves propagate in the z direction. Thus, the constructed CM is effectively uniaxial for the normal incidence wave.

For the structure shown in figure 3, when a linearly polarized wave with the E field in the x direction is incident in the z direction, the E field of the transmitted wave can be found in both the x and y directions, i.e., t_{xx} and t_{yx}. At the same time, the reflected wave is still linearly polarized in the x direction. On the basis of these scattering results, the reflection and transmission intensity spectra for RCP and LCP waves, the absorption spectra, the polarization azimuth rotation angle θ, and the ellipticity angle η of the transmitted wave can be calculated. In the following parts of the paper, for the purpose of clarity, only simulation results will be shown, since they are in good agreement with the corresponding experimental results. Figure 4 shows the simulation results corresponding to the structure of figure 3 [36].

On the basis of the transmission and reflection coefficients of RCP and LCP waves, the effective parameters $(n_+, n_-, n_0, \kappa, \varepsilon, \mu)$ can be retrieved, as shown in figure 5.

Comparing figures 5(a), (b) and (c), (d), due to the relation of $n_\pm = n_0 \pm \kappa$, the strong chirality κ can push the refractive index of the RCP (LCP) wave to be negative around the resonant frequency of 5.1 (6.4) GHz as shown in figures 5(c), (d). It is noted from figure 5(f) that in the vicinity of 5.1 GHz, the imaginary part of the effective parameter μ shows negative values. This phenomenon is very common in the retrieval process due to the inhomogeneity and the finite thickness of the unit cell [68].

The mechanism of the chiral metamaterial composed of four U-shaped resonators has been discussed in [36],
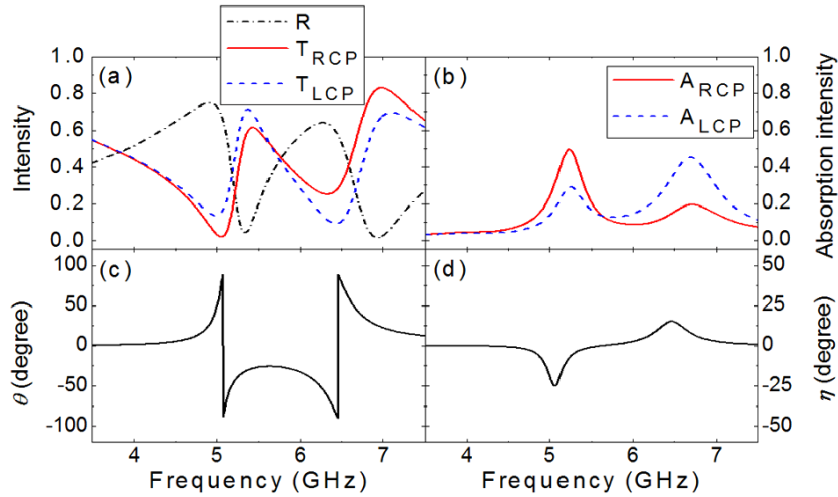
Figure 4. Simulation results for the chiral metamaterial of figure 3. (a) The intensity spectra of reflection and transmission for RCP and LCP waves. (b) The absorption spectra for RCP and LCP waves. (c) The polarization azimuth rotation angle θ. (d) The ellipticity angle η of the transmitted wave [36]. Reproduced with permission from [36]. © 2010 AIP.
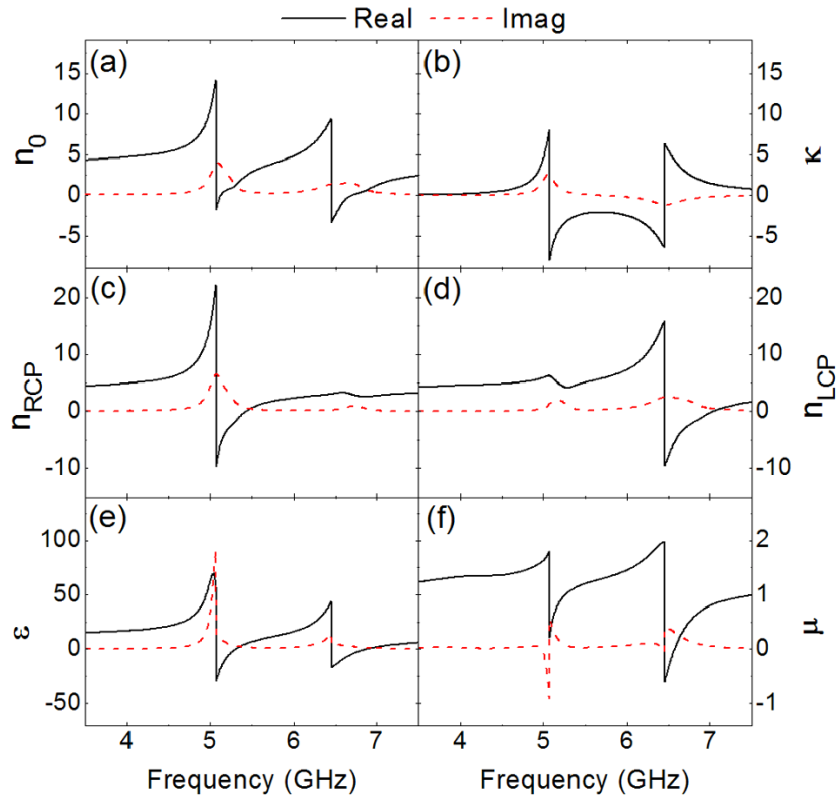
Figure 5. The retrieved effective parameters of the chiral metamaterials based on the simulation data. ((a), (b)) The refractive index n_0 and chirality κ. ((c), (d)) The refractive indices for RCP and LCP waves. ((e), (f)) The permittivity ε and permeability μ [36]. Reproduced with permission from [36]. © 2010 AIP.

by studying the current modes at resonances. A U-shaped resonator at resonance can be seen as an electric dipole in the plane coupled to a magnetic dipole perpendicular to the plane [67]. Since the two layers of U-shaped resonators are twisted by 90 degrees, all pairs of resonators can couple to each other only through the magnetic dipoles. At the lower resonant frequency of 5.1 GHz, the currents on the top and bottom four-U-SRRs are in the same direction, so the magnetic dipoles are parallel. In contrast, at the higher resonant frequency of 6.3 GHz, the currents on the top and bottom are in opposite directions, so the magnetic dipoles are antiparallel. According to the current distributions, when the chiral metamaterial is driven by the electric field in the x direction at 5.1 and 6.3 GHz, the x component of the induced
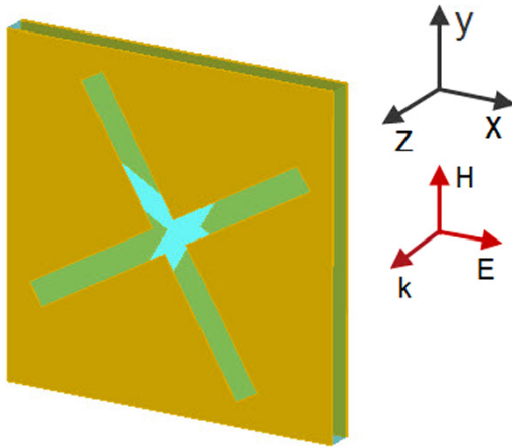
Figure 6. Schematic of a unit cell of the complementary cross-wire pair metamaterial. These cross-wire shaped slits are etched on the copper plates on the opposite sides of the FR-4 board [38]. Reproduced with permission from [38]. © 2011 AIP.

Figure 7. Simulation results for the complementary CM. (a) shows the transmission spectra for RCP and LCP waves. (b) shows the rotation angle θ and the ellipticity angle η of the transmitted wave [38]. Reproduced with permission from [38]. © 2011 AIP.

magnetic field H_x is nonzero. And, moreover, at 5.1 GHz, H_x and E_x are in opposite directions, while at 6.3 GHz, they are in the same direction [36]. This causality between electric and magnetic fields is consistent with the constitutive equation, equation (1).

3.2. Complementary chiral metamaterials with a negative refractive index

According to Babinet's principle [65], if the metal wire is normally illuminated from $z < 0$ by an incident field (E^0, B^0) and its complementary screen is illuminated by a complementary incident field $(E_c^0 = -cB^0, B_c^0 = E^0/c)$, then the pattern of the field scattered by the metal wire is the same as that which is scattered by its complement except that the polarization of the fields will be opposite for the two systems. Since the field scattered by the wire can be approximated as the radiation field by an electric dipole when the higher order multipolar fields are negligible, the field scattered by its complement can then be thought of as the radiation field produced by a virtual magnetic dipole. Babinet's principle has been applied in the design of metasurfaces and single-layered metamaterials [69, 70]. However, Babinet's principle cannot be applied directly to a bilayered structure. Consequently, this principle is rarely seen to be used to construct multilayered metamaterials. In this subsection, we introduce a novel design of a complementary chiral metamaterial based on the bilayered cross-wire chiral metamaterials [31, 38].

Figure 6 shows the schematic of one periodic unit cell of the complementary CM which consists of double-layered metal (copper) plates patterned on opposite sides of an FR-4 board. Two cross-wires that are mutually twisted by 30° are cut out from the two metal plates [38]. The structure is periodic in the x and y directions with both of the periodic constants being 21 mm—that is, less than the operating wavelength—and the thickness of the structure is 1.66 mm. The waves propagate in the z direction.

Using a procedure similar to those of section 3.1, the transmission spectra for RCP and LCP waves, the polarization
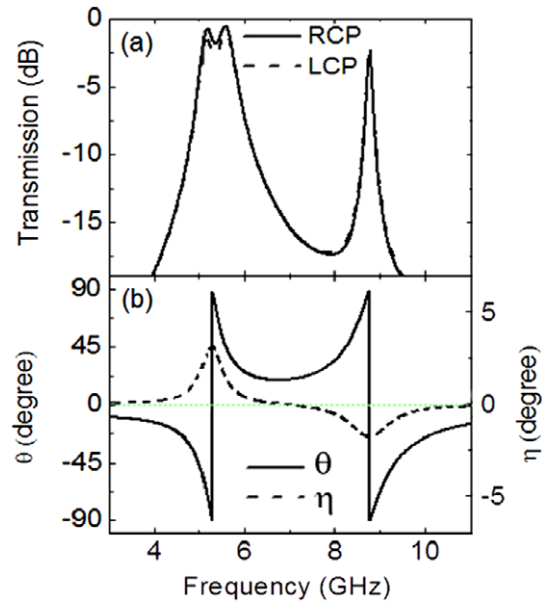
azimuth rotation angle θ, and the ellipticity angle η of the transmitted wave can be calculated. Figure 7 shows the simulation results. Figure 8 shows the retrieved effective parameters ($n_+, n_-, n_0, \kappa, \varepsilon, \mu$).

On the κ curves shown in figure 8(b), there are two resonances related to the chirality. The lower frequency resonance happens at $f = 5.28$ GHz, and the upper one happens at $f = 8.77$ GHz. Below $f = 5.28$ GHz, n_0 is positive while κ is negative. Above this frequency, n_0 is negative and κ is positive. For $f = 8.77$ GHz, only κ changes its sign while n_0 remains positive on both sides. Comparing figures 8(a), (b) and (c), (d), due to the relation of $n_\pm = n_0 \pm \kappa$, the strong chirality κ has pushed the refractive index of the RCP wave from positive to negative values below $f = 5.28$ GHz and above $f = 8.77$ GHz. At the same time, above $f = 5.28$ GHz, the originally negative index band of the LCP wave becomes wider. Figures 8(e), (f) show the retrieved results for ε and μ. It is noteworthy that in the frequency ranges 5.10–5.28 and 8.77–8.90 GHz, both Re(μ) and Re(ε) are positive and will not result in a negative index in traditional metamaterials. Therefore, the negative index of the RCP wave is actually attributed to the relatively small n_0 and the large chirality κ. Like for the case of figure 5(f), there are regions where the imaginary part of μ has negative values.

In order to understand the mechanism of the chiral behaviors, the distributions of the H fields on the middle plane between the two metal plates and the surface current modes at resonances have been studied [38]. Figure 9 shows the simulated H field distributions and the current modes at the frequencies of two transmission peaks, e.g., figures 9(a) and (b) at $f_1 = 5.17$ GHz, and figures 9(c) and (d) at $f_2 = 5.58$ GHz, respectively. For both cases, the incident waves have the E field polarized in the x direction. From figures 9(a)
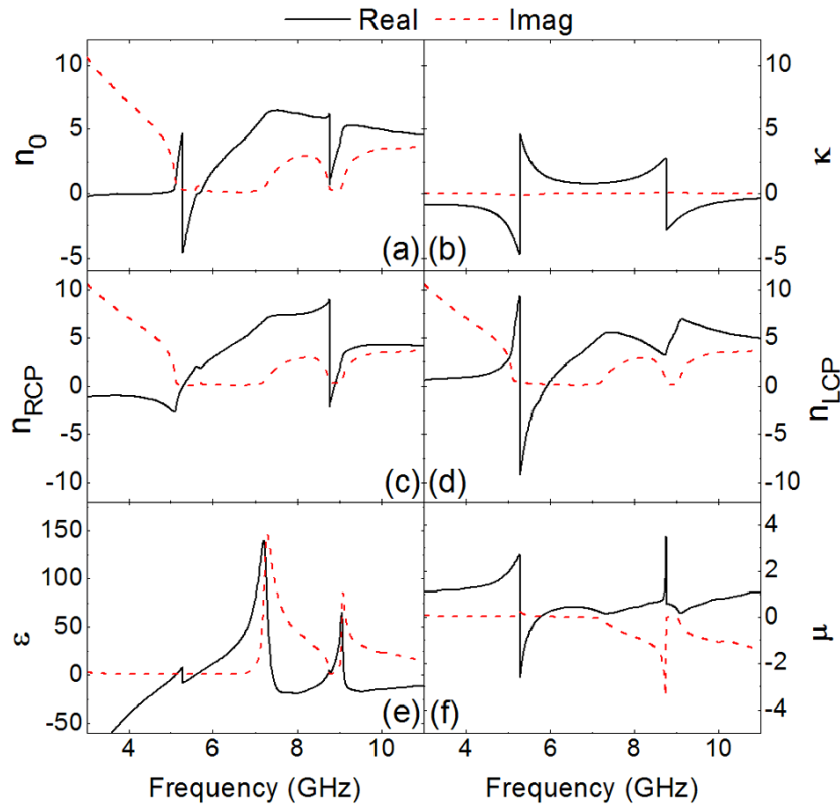
Figure 8. The retrieved effective parameters of the complementary CM based on the simulation data. ((a), (b)) The refractive index n_0 and chirality κ. ((c), (d)) The refractive indices for RCP and LCP waves. ((e), (f)) The permittivity ε and permeability μ [38]. Reproduced with permission from [38]. © 2011 AIP.
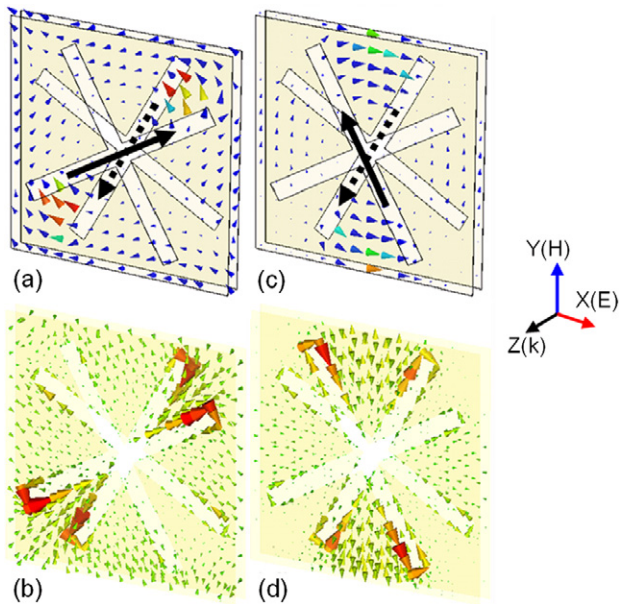
Figure 9. The scattered H field distributions on the middle plane between the two metal plates and the current modes when driven by the incident field with E in the x direction at ((a) and (b)) 5.17 GHz and ((c) and (d)) 5.58 GHz. The long solid (dashed) arrows represent the front (back) virtual magnetic dipoles [38]. Reproduced with permission from [38]. © 2011 AIP.

and (b), one sees that the distributions of the H field and the current mode both resemble the case for the coupling of a pair of antisymmetrically arranged magnetic dipoles. The

two virtual magnetic dipoles are depicted in figure 9(a), with the thick solid (dashed) arrow representing the front (back) virtual magnetic dipole. The angle is 30° between the two dipoles. For the case of figures 9(c) and (d), the distributions of the H field and current mode also resemble the case for the coupling of a pair of antisymmetrically arranged magnetic dipoles. The only difference is the angle, which is 60° in this case. At the higher resonant frequency of 8.77 GHz, the H field distribution and the current mode do not resemble those of magnetic dipoles [38]. These interesting phenomena indicate that Babinet's principle can really be applied in the design of bilayered complementary chiral metamaterials at lower resonant frequencies.

3.3. Composite chiral metamaterial with a negative refractive index and high value of the figure of merit

So far, quite a few negative index CMs have been reported [29–38]. However, it was found that, except for the complementary CMs as discussed in section 3.2, when a large chirality κ is obtained, a large relative permittivity ε (or large relative permeability μ) coexists below the frequency of chiral resonances. Consequently, the absolute value of the chirality κ is always less than n_0 in the frequency range below the chiral resonances. Therefore, the negative index can only happen in the frequency range above the resonance, where the relative permittivity ε (or relative permeability μ) is very low and/or even in the negative region. Consequently, a composite CM
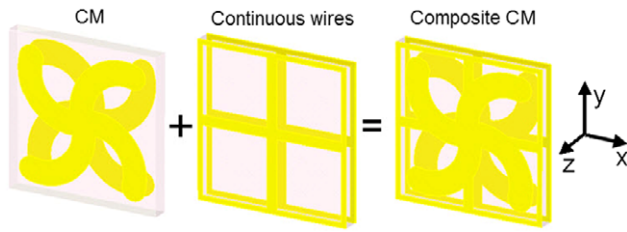
Figure 10. The schematics of the construction of the composite CM by the combination of a CM and a structure of continuous metallic wires [41]. Reproduced with permission from [41]. © 2012 OSA.

that consists of chiral components and continuous metallic wires was proposed [41]. By using continuous metallic wires, the large permittivity below the resonance is partially compensated, which makes n_0 become smaller than κ below the frequency of resonance. Therefore, a negative index can be realized in the frequency region below the chiral resonances.

Figure 10 shows the schematics of the construction of the unit cell of the composite CM [41]. The copper conjugated rosettes and continuous wires are patterned on the opposite sides of a Teflon dielectric board. The structure is periodic in the x and y directions with both of the periodic constants being 19 mm—that is, less than the operating wavelength—and the thickness of the structure is 2.06 mm. The waves propagate in the z direction. In order to study the effect of additional continuous metallic wires on the CM structure that only consists of conjugated rosettes, both the CM and the composite CM were investigated, in comparison.

Figure 11 shows the retrieved effective parameters for one layer of the CM and composite CM (the real and imaginary parts of n_+, n_-) based on the simulation data. For the CM, due to the high value of ε and/or μ below the resonant frequencies (see figure 3 of [41]), one cannot obtain a negative index below the resonant frequencies. Furthermore, in the regions just above the frequency of the chiral resonances, both n_+ and n_- possess a high value for the imaginary part. Therefore, the FOM of the negative refractive index deteriorates in these regions. Only those small regions that are indicated by shadowed regions in figures 11(a) and (c) can be useful in the construction of negative index chiral metamaterials. For the RCP wave, this useful negative index band is from 9.56 to 9.71 GHz, and the maximum figure of merit is 8.4. For the LCP wave, the useful negative index band is from 4.42 to 4.53 GHz, and the maximum figure of merit reaches 6.6.

Figures 11(b) and (d) show the retrieved parameters for the composite CM. For the RCP wave, the negative index band still lies above the resonant frequency. The regions of negative index, where the imaginary part is small, are indicated with shadows. In particular, in the frequency range from 5.36 to 5.58 GHz, the maximum figure of merit can reach more than 50. For the LCP wave, there is a negative index band (from 5.13 to 5.29 GHz) below the resonant frequency, and the maximum figure of merit reaches 18. In figures 11(b) and (d), one sees very large values of the imaginary parts of the effective indices in the left and right boundaries of the frequency band studied. This is due to the existence of the continuous metallic wires and the two resonances at 5.36 and

8.7 GHz that pushed the effective parameter of ε below zero in the vicinity of these two frequencies, and more details can be found from figures 5–7 in [41].

Obviously, the figure of merit of the composite CM is much larger than that of the CM. The above results show that the composite CMs may be a better choice for the construction of negative index CMs.

## 4. Construction of bulk chiral metamaterials

Theoretical works showed that isotropic CMs can be constructed by stacking chiral unit cells in a 3D periodic lattice [15, 71]. It was also demonstrated experimentally for the microwave regime that a two-dimensional CM can be constructed with a nonplanar chiral unit cell [19, 20]. For planar CMs, a straightforward way to construct a bulk CM is to stack them layer by layer periodically. However, when one tries to construct a bulk CM in this way, the situation may become complex because the building blocks can strongly interact. One must, therefore, investigate how the effective parameters change when the interaction between these chiral units is strong.

Figure 12(a) shows the schematic for a stack of two layers of planar chiral units that are composed of twisted cross-wires [39]. The structure is periodic in the x and y directions with both of the periodic constants being 13 mm—that is, less than the operating wavelength—and the thickness of each layer of chiral structure is 1.06 mm. The waves propagate in the z direction. The four cross-wires are labeled from w1 to w4. Obviously, there are coupling effects between the cross-wire pair of w1 and w2 and the pair of w3 and w4 that make each unit cell a chiral one. When the two unit cells are placed near each other, there exist additional coupling effects. One kind of coupling effect comes from the coupling between the cross-wires of w1 (w2) and w3 (w4). This kind of coupling does not contribute to the optical activity, but it may affect the impedance of the whole structure. The other kind of coupling effect comes from the coupling between the cross-wires of w1 (w2) and w4 (w3). In particular, due to the relatively small distance between w2 and w3, as shown in figure 12(b), the coupling between them can greatly change the optical activity of the whole structure. As shown in [39], when the distance between the adjacent chiral layers is small, the effective parameters of the bulk CM can be very different from the parameters of a single layer of CM.

Therefore, during the designing of a bulk CM by stacking chiral units in a periodic lattice, if there are effects of coupling between the unit cells, an approximate analytical theory based on the Lorentz homogenization procedure [15, 71] may not be enough, while rigorous full-wave electromagnetic simulations must be carried out in order to identify the eigenmodes of the bulk structure.

5. Asymmetric transmissions achieved with deformed chiral metamaterials

Although a uniaxial chiral metamaterial is usually preferred for application, sometimes an anisotropic chiral structure can also provide interesting properties, e.g., acting as a circular
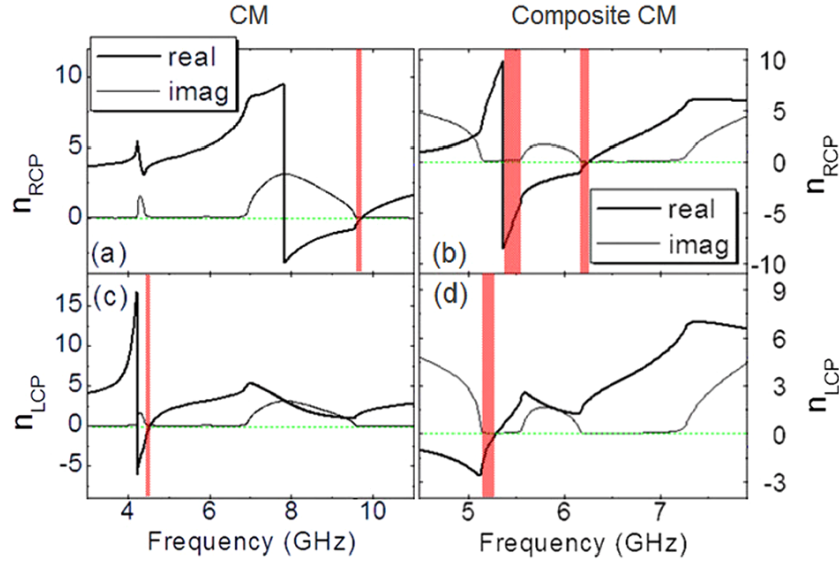
Figure 11. The retrieved effective parameters of the CM and composite CM based on the simulation data. (a)–(d) show the real and imaginary parts of the refractive index of RCP and LCP waves for the CM and composite CM, respectively. The shadowed regions show the negative index bands with small imaginary parts and high values of the figure of merit [41]. Reproduced with permission from [41]. © 2012 OSA.
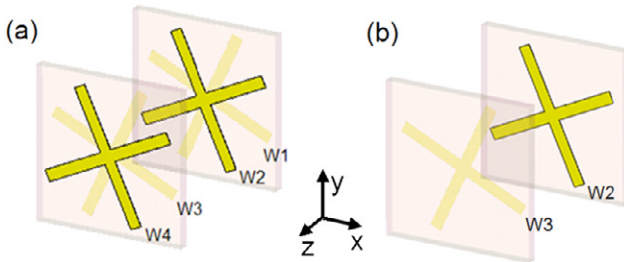
Figure 12. (a) Schematic of a chiral metamaterial obtained by stacking two layers of planar chiral structures. (b) Schematic showing the coupling between two cross-wires belonging to two unit cells [39]. Reproduced with permission from [39]. © 2010 OSA.

polarizer [72] and achieving asymmetric transmissions [62, 63]. In this section, we would like to introduce the interesting phenomenon of asymmetric transmissions by using deformed chiral structures.

The transmission of coherent electromagnetic waves through a dispersive medium that is embedded in vacuum or air can be described by means of complex Jones matrices T. Consider a normally incident plane wave propagating in the $+z$ direction $E_i(r, t) = (I_x, I_y)^T e^{i(kz-\omega t)}$, with frequency ω, wavevector k, and complex amplitudes I_x and I_y in the x and y directions, respectively. The transmitted wave is given by $E_t(r, t) = (T_x, T_y)^T e^{i(kz-\omega t)}$. The complex amplitudes of the incident waves can be related to that of transmitted waves by the T matrix [61, 73],

$$\begin{pmatrix} T_x \\ T_y \end{pmatrix} = \begin{pmatrix} T_{xx} & T_{xy} \\ T_{yx} & T_{yy} \end{pmatrix} \begin{pmatrix} I_x \\ I_y \end{pmatrix} = \begin{pmatrix} A & B \\ C & D \end{pmatrix} \begin{pmatrix} I_x \\ I_y \end{pmatrix} = \hat{T}_{\text{lin}}^{\text{f}} \begin{pmatrix} I_x \\ I_y \end{pmatrix}. \tag{13}$$

The index f indicates the forward propagation, while lin indicates the linear base with the base vectors parallel to the coordinate axes, i.e., the incident and transmitted waves are

decomposed into the x and y polarized waves. For the fixed coordinate system, the wave propagation in the backward direction is defined as the situation where the sample is rotated by 180° with respect to either the x or the y axis. For a medium made of reciprocal materials, applying the reciprocity theorem of four-port systems yields the T matrix $\hat{T}_{\text{lin}}^{b}$, [61, 73]:

$$\hat{T}_{\text{lin}}^{b} = \begin{pmatrix} A & -C \\ -B & D \end{pmatrix}. \tag{14}$$

These components (A, B, C, and D) obey fixed relations for certain symmetries of the medium. For example, for the planar chiral structures, due to the existence of mirror symmetry perpendicular to the propagation direction, the component B is equal to C and, therefore,

$$\hat{T}_{\text{lin}}^{\text{f}} = \begin{pmatrix} A & B \\ B & D \end{pmatrix}, \qquad \hat{T}_{\text{lin}}^{b} = \begin{pmatrix} A & -B \\ -B & D \end{pmatrix}. \tag{15}$$

On the other hand, for a uniaxial chiral structure, due to the existence of the C4 symmetry with respect to the z axis, the component A is equal to D and C is equal to $-B$ and, therefore,

$$\hat{T}_{\text{lin}}^{\text{f}} = \hat{T}_{\text{lin}}^{b} = \begin{pmatrix} A & B \\ -B & A \end{pmatrix}. \tag{16}$$

From equations (13) and (14), the asymmetric transmission for a given linear base vector can be defined as the difference between the transmitted intensities for different propagation directions as

$$\Delta_{\text{lin}}^{(x)} = (|A|^2 + |C|^2) - (|A|^2 + |B|^2) = |C|^2 - |B|^2$$
$$= (|D|^2 + |C|^2) - (|D|^2 + |B|^2) = -\Delta_{\text{lin}}^{(y)}. \tag{17}$$

From equations (15) and (16), it is clear that planar chiral structures and uniaxial chiral structures cannot produce

9
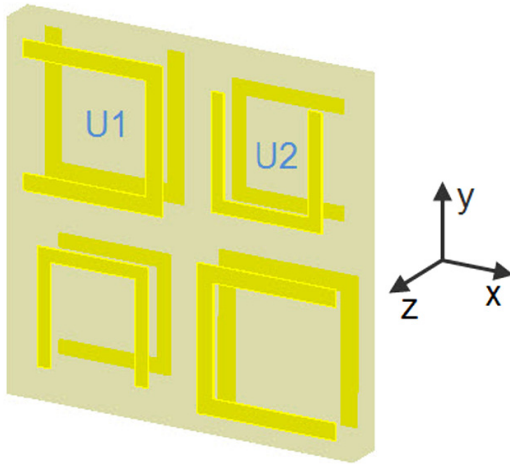
Figure 13. Schematic of a deformed chiral structure for achieving an asymmetric transmission of linearly polarized incident waves. The U1 and U2 split ring resonators have different dimensions [62]. Reproduced with permission from [62]. © 2011 OSA.

asymmetric transmissions for linearly polarized incident waves. To achieve asymmetric transmission for linearly polarized incident waves, one approach is to break the mirror symmetry perpendicular to the propagation direction based on the planar chiral structure, such as the 3D structure proposed by Menzel *et al* [61]. The other approach is to break the C4 rotation symmetry of the uniaxial chiral structures [62, 63], which is what we are going to introduce in the following.
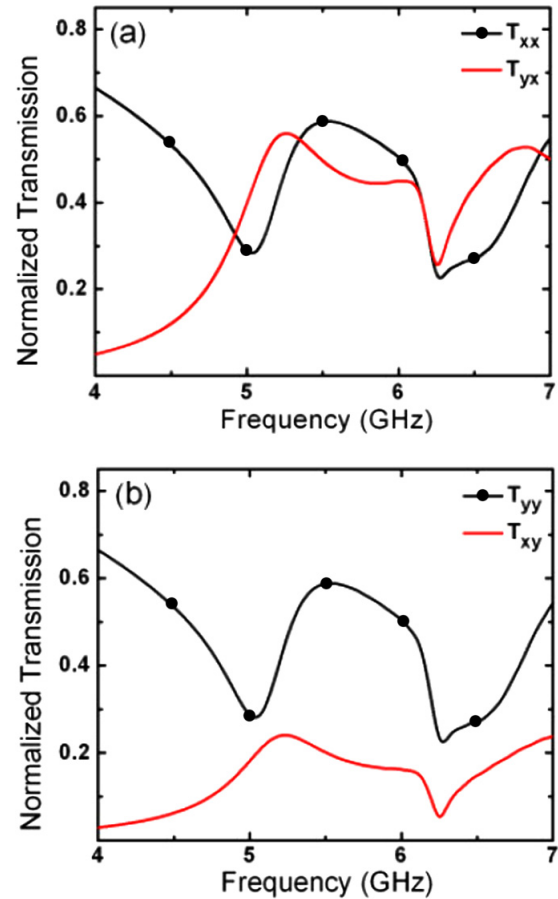
5.1. Asymmetric transmission based on a deformed chiral structure

Taking the uniaxial chiral structure of figure 3, for instance, one method of breaking the C4 rotation symmetry of the uniaxial chiral structures is to make the whole structure consist of U-shaped split ring resonators with different dimensions, as demonstrated by Mehmet *et al* [62].

Figure 13 shows the schematic of a deformed chiral structure that is composed of different sized U-shaped split ring resonators [62]. The structure is periodic in the x and y directions with both of the periodic constants being 13.6 mm—that is, less than the operating wavelength—and the thickness of the structure is 1.56 mm. The waves propagate in the z direction. After the breaking of the C4 rotational symmetry, the T matrices of the structure now have the following form:

$$\hat{T}_{\text{lin}}^{\text{f}} = \begin{pmatrix} A & B \\ C & A \end{pmatrix}, \qquad \hat{T}_{\text{lin}}^{b} = \begin{pmatrix} A & -C \\ -B & A \end{pmatrix}. \qquad (18)$$

Figure 14 shows the simulation results for the transmission coefficients for x and y polarized incident waves. The results in figure 14 are in agreement with equation (18). Due to the different transmission amplitudes of T_{yx} and T_{xy}, asymmetric transmission can be realized for linearly polarized incident waves [62].

Figure 14. (a) Simulation results for the linear transmission coefficients when the deformed chiral structure is illuminated by (a) x-polarized and (b) y-polarized incident waves [62]. Reproduced with permission from [62]. © 2011 OSA.

5.2. Asymmetric transmission using a deformed chiral structure and electromagnetic wave tunneling

Although the structure of figure 13 can provide asymmetric transmissions for linearly polarized incident waves, the extent of this asymmetric transmission is not very good because of the existence of the high transmission amplitudes of T_{xx} and T_{yy}. In an ideal asymmetric transmission, in one direction the transmission is unity while in the opposite direction the transmission is zero. This requires the diagonal components of the T matrix to be zero, and one of the off-diagonal components to be zero while the other is unity, such that

$$\hat{T}_{\text{lin}}^{\text{f}} = \begin{pmatrix} 0 & 1 \\ 0 & 0 \end{pmatrix}, \qquad \hat{T}_{\text{lin}}^{b} = \begin{pmatrix} 0 & 0 \\ -1 & 0 \end{pmatrix}. \qquad (19)$$

According to this idea, a structure consisting of a deformed chiral structure and a continuous wire structure was proposed for accomplishing this task [63].

Figure 15 shows the proposed structure [63]. This structure consists of a deformed chiral structure similar to that of figure 13 and an additional structure with continuous wires. The structure is periodic in the x and y directions with both of the periodic constants being 12.8 mm—that is, less than
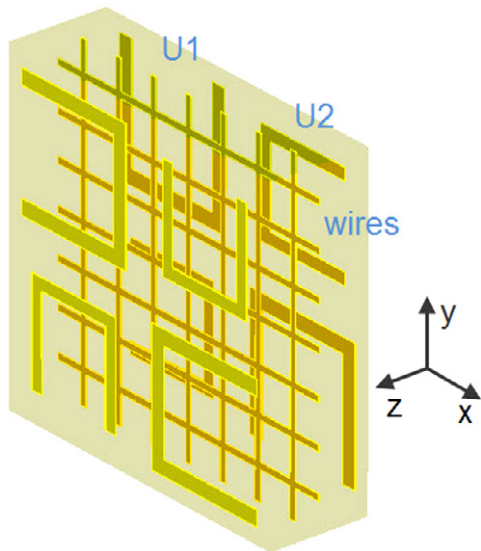
Figure 15. Schematic of the structure consisting of a continuous wire structure sandwiched between two sets of U-shaped resonators for achieving the asymmetric transmission of linearly polarized incident waves. The U1 and U2 split ring resonators have different dimensions [63]. Reproduced with permission from [63]. © 2012 APS.

the operating wavelength—and the thickness of the structure is 2.06 mm. The waves propagate in the z direction. Due to the presence of the additional continuous wire structure, which can effectively provide negative permittivity in the x and y directions for the whole structure, the transmissions of T_{xx} and T_{yy} are greatly depressed in a selected frequency range. However, this additional continuous wire structure has very little effect on the permittivity or permeability in the z direction. Therefore, the coupling between the magnetic dipoles of the U-shaped resonator pairs still exists, which provides the tunneling effect for the transmission of T_{xy} and of T_{yx} [63, 74]. Then, by tuning the geometric dimensions of the resonators, T_{yx} is depressed in the selected frequency range while at the same time T_{xy} retains high values. Consequently, a diode-like asymmetric transmission for x polarized incident waves is realized, as shown in figure 16.

6. Conclusions

In this review, we have assessed recent progress in the field of chiral metamaterials. Then, on the basis of the related studies of the authors' group, we primarily introduced some typical chiral metamaterials that comprise bilayered planar meta-atoms, e.g., chiral metamaterials consisting of U-shaped split ring resonators, complementary chiral metamaterials, and composite chiral metamaterials designed to achieve high figure of merit values with a negative refractive index. We also mentioned the construction of bulk chiral metamaterials and the related possible problems when there are strong effects of coupling between adjacent chiral unit cells. After breaking the C4 circular rotation symmetry of a uniaxial chiral metamaterial, a bianisotropic chiral structure can be obtained that can show interesting properties, such as acting as a circular polarizer and providing asymmetric transmissions for linearly polarized incident waves.
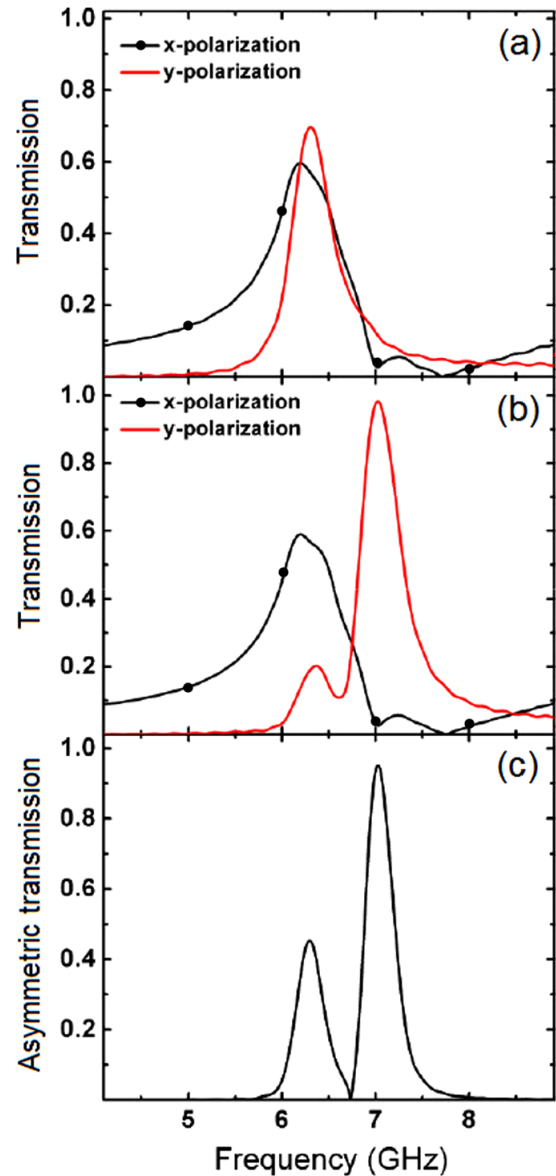
Figure 16. Simulation results for transmission spectra for the structure of figure 15: (a) and (b) are for x-polarized forward and backward incident waves, respectively. (c) shows the spectrum of asymmetric transmission [63]. Reproduced with permission from [63]. © 2012 APS.

Giant optical activity, circular dichroism, and a negative refractive index due to chirality have been demonstrated for the microwave and terahertz regimes [18, 19, 29, 31]. Although giant optical activity and circular dichroism have also been achieved for infrared and visible frequencies [32, 35], chiral metamaterials with a negative refractive index have not been realized in this frequency regime yet. Although it has been proposed that chiral metamaterials with a negative refractive index can be used to focus circularly polarized waves, experiments are needed to demonstrate the focusing effect. Apart from exhibiting properties such as giant optical activity, circular dichroism, and a negative refractive index, chiral metamaterials were also shown to be able to act as absorbers [20], and even to affect the Casimir forces [75–77].

We hope that more exotic designs and applications involving chiral metamaterials will be developed in the future.

References

[1] Smith D R, Padilla W J, Vier D C, Nemat-Nasser S C and Schultz S 2000 A composite medium with simultaneously negative permeability and permittivity *Phys. Rev. Lett.* **84** 4184–7

[2] Pendry J B, Holden A J, Stewart W J and Youngs I 1996 Extremely low frequency plasmons in metallic mesostructures *Phys. Rev. Lett.* **76** 4773–6

[3] Pendry J B, Holden A J, Robbins D J and Stewart W J 1999 Magnetism from conductors and enhanced nonlinear phenomena *IEEE Trans. Microw. Theory Tech.* **47** 2075–84

[4] Dolling G, Enkrich C, Wegener M, Zhou J F, Soukoulis C M and Linden S 2005 Cut-wire pairs and plate pairs as magnetic atoms for optical metamaterials *Opt. Lett.* **30** 3198–200

[5] Kafesaki M, Tsiapa I, Katsarakis N, Koschny T, Soukoulis C M and Economou E N 2007 Left-handed metamaterials: the fishnet structure and its variations *Phys. Rev. B* **75** 235114

[6] Aydin K, Li Z, Sahin L and Ozbay E 2008 Negative phase advance in polarization independent, multi-layer negative-index metamaterials *Opt. Express* **16** 8835–44

[7] Shalaev V M 2007 Optical negative-index metamaterials *Nature Photon.* **1** 41–8

[8] Zhou J, Koschny T, Kafesaki M, Economou E N, Pendry J B and Soukoulis C M 2005 Saturation of magnetic response of split-ring resonators at optical frequencies *Phys. Rev. Lett.* **95** 223902

[9] Pendry J B 2004 A chiral route to negative refraction *Science* **306** 1353–5

[10] Tretyakov S, Nefedov I, Sihvola A, Maslovski S and Simovski C 2003 Waves and energy in chiral nihility *J. Electromagn. Waves Appl.* **17** 695–706

[11] Tretyakov S, Sihvola A and Jylha L 2005 Backward-wave regime and negative refraction in chiral composites *Photon. Nanostruct. Fundam. Appl.* **3** 107–15

[12] Monzon C and Forester D W 2005 Negative refraction and focusing of circularly polarized waves in optically active media *Phys. Rev. Lett.* **95** 123904

[13] Jin Y and He S 2005 Focusing by a slab of chiral medium *Opt. Express* **13** 4974–9

[14] Yannopapas V 2006 Negative index of refraction in artificial chiral materials *J. Phys.: Condens. Matter* **18** 6883–90

[15] Jelinek L, Marques R, Mesa F and Baena J D 2008 Periodic arrangements of chiral scatterers providing negative refractive index bi-isotropic media *Phys. Rev. B* **77** 205110

[16] Bose J C 1898 On the rotation of plane of polarisation of electric waves by a twisted structure *Proc. R. Soc.* **63** 146–52

[17] Lindell I V, Sihvola A H and Kurkijarvi J 1992 Karl F Lindman: the last hertzian, and a harbinger of electromagnetic chirality *IEEE Antennas Propag. Mag.* **34** 24–30

[18] Zhang S, Park Y S, Li J, Lu X, Zhang W and Zhang X 2009 Negative refractive index in chiral metamaterials *Phys. Rev. Lett.* **102** 023901

[19] Wang B, Zhou J, Koschny T and Soukoulis C M 2009 Nonplanar chiral metamaterials with negative index *Appl. Phys. Lett.* **94** 151112

[20] Wang B, Koschny T and Soukoulis C. M 2009 Wide-angle and polarization-independent chiral metamaterial absorber *Phys. Rev. B* **80** 033108

[21] Papakostas A, Potts A, Bagnall D M, Prosvirnin S L, Coles H J and Zheludev N I 2003 Optica manifestations of planar chirality *Phys. Rev. Lett.* **90** 177401

[22] Vallius T, Jefimovs K, Turunen J, Vahimaa P and Svirko Y 2003 Optical activity in subwavelength-period arrays of chiral metallic particles *Appl. Phys. Lett.* **83** 234–6

[23] Kuwata-Gonokami M, Saito N, Ino Y, Kauranen M, Jefimovs K, Vallius T, Turunen J and Svirko Y 2005 Giant optical activity in quasi-two-dimensional planar nanostructures *Phys. Rev. Lett.* **95** 227401

[24] Bai B, Svirko Y, Turunen J and Vallius T 2007 Optical activity in planar chiral metamaterials: theoretical study *Phys. Rev. A* **76** 023811

[25] Arnaut L R and Davis L E 1995 On planar chiral structures *Progress in Electromagnetic Research Symp. PIERS; (Seattle WA, 1995)* p 165

[26] Arnaut L R 1997 Chirality in multi-dimensional space with application to electromagnetic characterisation of multi-dimensional chiral and semi-chiral media *J. Electromagn. Waves Appl.* **11** 1459–82

[27] Prosvirnin S L and Zheludev N I 2005 Polarization effects in the diffraction of light by a planar chiral structure *Phys. Rev. E* **71** 037603

[28] Rogacheva A V, Fedotov V A, Schwanecke A S and Zheludev N I 2006 Giant gyrotropy due to electromagnetic-field coupling in a bilayered chiral structure *Phys. Rev. Lett.* **97** 177401

[29] Plum E, Zhou J, Dong J, Fedotov V A, Koschny T, Soukoulis C M and Zheludev N I 2009 Metamaterial with negative index due to chirality *Phys. Rev. B* **79** 035407

[30] Plum E, Fedotov V A, Schwanecke A S and Zheludev N I 2007 Giant optical gyrotropy due to electromagnetic coupling *Appl. Phys. Lett.* **90** 223113

[31] Zhou J, Dong J, Wang B, Koschny T, Kafesaki M and Soukoulis C M 2009 Negative refractive index due to chirality *Phys. Rev. B* **79** 121104

[32] Decker M, Ruther M, Kriegler C E, Zhou J, Soukoulis C M, Linden S and Wegener M 2009 Strong optical activity from twisted-cross photonic metamaterials *Opt. Lett.* **34** 2501–3

[33] Ye Y and He S 2010 90° polarization rotator using a bilayered chiral metamaterial with giant optical activity *Appl. Phys. Lett.* **96** 203501

[34] Zhao R, Zhang L, Zhou J, Koschny T and Soukoulis C M 2011 Conjugated gammadion chiral metamaterial with uniaxial optical activity and negative refractive index *Phys. Rev. B* **83** 035105

[35] Decker M, Zhao R, Soukoulis C M, Linden S and Wegener M 2010 Twisted split-ring-resonator photonic metamaterial with huge optical activity *Opt. Lett.* **35** 1593–5

[36] Li Z F, Zhao R, Koschny T, Kafesaki M, Alici K B, Colak E, Caglayan H, Ozbay E and Soukoulis C M 2010 Chiral metamaterials with negative refractive index based on four 'U' split ring resonators *Appl. Phys. Lett.* **97** 081901

[37] Xiong X, Sun W H, Bao Y J, Wang M, Peng R W, Sun C, Lu X, Shao J, Li Z F and Ming N B 2010 Construction of a chiral metamaterial with a U-shaped resonator assembly *Phys. Rev. B* **81** 075119

[38] Li Z F, Alici K B, Colak E and Ozbay E 2011 Complementary chiral metamaterials with giant optical activity and negative refractive index *Appl. Phys. Lett.* **98** 161907

[39] Li Z F, Caglayan H, Colak E, Zhou J, Soukoulis C M and Ozbay E 2010 Coupling effect between two adjacent chiral structure layers *Opt. Express* **18** 5375–83

[40] Soukoulis C M and Wegener M 2011 Past achievements and future challenges in the development of three-dimensional photonic metamaterials *Nature Photon.* **5** 523–30

[41] Li Z F, Alici K B, Caglayan H, Kafesaki M, Soukoulis C M and Ozbay E 2012 Composite chiral metamaterials with negative refractive index and high values of the figure of merit *Opt. Express* **20** 6146–56

[42] Zhou J, Chowdhury D R, Zhao R, Azad A K, Chen H T, Soukoulis C M, Taylor A J and O'Hara J F 2012 Terahertz chiral metamaterials with giant and dynamically tunable optical activity *Phys. Rev.* B **86** 035448

[43] Smith D R, Schultz S, Markos P and Soukoulis C M 2002 Determination of effective permittivity and permeability of metamaterials from reflection and transmission coefficients *Phys. Rev.* B **65** 195104

[44] Prosvirnin S L and Zouhdi S 2006 On the effective constitutive parameters of metal–dielectric arrays of complex-shaped particles *J. Electromagn. Waves Appl.* **20** 583–98

[45] Li Z F, Aydin K and Ozbay E 2009 Determination of the effective constitutive parameters of bianisotropic metamaterials from reflection and transmission coefficients *Phys. Rev.* E **79** 026610

[46] Li Z F, Aydin K and Ozbay E 2010 Transmission spectra and the effective parameters for planar metamaterials with omega shaped metallic inclusions *Opt. Commun.* **282** 2547–51

[47] Li Z F, Aydin K and Ozbay E 2012 Retrieval of effective parameters for bianisotropic metamaterials with omega shaped metallic inclusions *Photon. Nanostruct. Fundam. Appl.* **10** 329–36

[48] Kwon D H, Werner D H, Kildishev A V and Shalaev V M 2008 Material parameter retrieval procedure for general bi-isotropic metamaterials and its application to optical chiral negative-index metamaterial design *Opt. Express* **16** 11822–9

[49] Menzel C, Rockstuhl C, Paul T and Lederer F 2008 Retrieving effective parameters for quasiplanar chiral metamaterials *Appl. Phys. Lett.* **93** 233106

[50] Zhao R, Koschny T and Soukoulis C M 2010 Chiral metamaterials: retrieval of the effective parameters with and without substrate *Opt. Express* **18** 14553–67

[51] Wang Z, Chong Y, Joannopoulos J D and Soljacic M 2009 Observation of unidirectional backscattering-immune topological electromagnetic states *Nature* **461** 772–5

[52] Tuz V R and Prosvirnin S L 2011 Bistability, multistability, and nonreciprocity in a chiral photonic bandgap structure with nonlinear defect *J. Opt. Soc. Am.* B **28** 1002–8

[53] Fan L, Wang J, Varghese L T, Shen H, Niu B, Xuan Y, Weiner A M and Qi M 2012 An all-silicon passive optical diode *Science* **335** 447–50

[54] Feng L, Ayache M, Huang J, Xu Y, Lu M, Chen Y, Fainman Y and Scherer A 2011 Nonreciprocal light propagation in a silicon photonic circuit *Science* **333** 729–33

[55] Serebryannikov A E 2009 One-way diffraction effects in photonic crystal gratings made of isotropic materials *Phys. Rev.* B **80** 155117

[56] Cakmakyapan S, Caglayan H, Serebryannikov A E and Ozbay E 2011 Experimental validation of strong directional selectivity in nonsymmetric metallic gratings with a subwavelength slit *Appl. Phys. Lett.* **98** 051103

[57] Prosvirnin S L and Zheludev N I 2009 Analysis of polarization transformations by a planar chiral array of complex-shaped particles *J. Opt. A: Pure Appl. Opt.* **11** 074002

[58] Fedotov V A, Mladyonov P L, Prosvirnin S L, Rogacheva A V, Chen Y and Zheludev N I 2006 Asymmetric propagation of electromagnetic waves through a planar chiral structure *Phys. Rev. Lett.* **97** 167401

[59] Fedotov V A, Schwanecke A S, Zheludev N I, Khardikov V V and Prosvirnin S L 2007 Asymmetric transmission of light and enantiomerically sensitive plasmon resonance in planar chiral nanostructures *Nano Lett.* **7** 1996–9

[60] Schwanecke A S, Fedotov V A, Khardikov V V, Prosvirnin S L, Chen Y and Zheludev N I 2008 Nanostructured metal film with asymmetric optical transmission *Nano Lett.* **8** 2940–3

[61] Menzel C, Helgert C, Rockstuhl C, Kley E B, Tunnermann A, Pertsch T and Lederer F 2010 Asymmetric transmission of linearly polarized light at optical metamaterials *Phys. Rev. Lett.* **104** 253902

[62] Mutlu M, Akosman A E, Serebryannikov A E and Ozbay E 2011 Asymmetric transmission of linearly polarized waves and polarization angle dependent wave rotation using a chiral metamaterial *Opt. Express* **19** 14290–9

[63] Mutlu M, Akosman A E, Serebryannikov A E and Ozbay E 2012 Diodelike asymmetric transmission of linearly polarized waves using magnetoelectric coupling and electromagnetic wave tunneling *Phys. Rev. Lett.* **108** 213905

[64] Kong J A 2008 *Electromagnetic Wave Theory* (Cambridge, MA: EMW Publishing)

[65] Jackson J D 1998 *Classical Electrodynamics* 3rd edn (New York: Wiley)

[66] Liu H, Genov D A, Wu D M, Liu Y M, Liu Z W, Sun C, Zhu S N and Zhang X 2007 Magnetic plasmon hybridization and optical activity at optical frequencies in metallic nanostructures *Phys. Rev.* B **76** 073101

[67] Liu N, Liu H, Zhu S N and Giessen H 2009 Stereometamaterials *Nature Photon.* **4** 157–62

[68] Koschny T, Markos P, Smith D R and Soukoulis C M 2003 Resonant and antiresonant frequency dependence of the effective parameters of metamaterials *Phys. Rev.* E **68** 065602

[69] Liu N, Kaiser S and Giessen H 2008 Magnetoinductive and electroinductive coupling in plasmonic metamaterial molecules *Adv. Mater.* **20** 4521–5

[70] Khardikov V V, Iarko E O and Prosvirnin S L 2010 Trapping of light by metal arrays *J. Opt.* **12** 045102

[71] Marques R, Jelinek L and Mesa F 2007 Negative refraction from balanced quasi-planar chiral inclusions *Microw. Opt. Technol. Lett.* **49** 2606–9

[72] Mutlu M, Akosman A E, Serebryannikov A E and Ozbay E 2011 Asymmetric chiral metamaterial circular polarizer based on four U-shaped split ring resonators *Opt. Lett.* **36** 1653–5

[73] Menzel C, Rockstuhl C and Lederer F 2010 Advanced Jones calculus for the classification of periodic metamaterials *Phys. Rev.* A **82** 053811

[74] Mutlu M and Ozbay E 2012 A transparent 90° polarization rotator by combining chirality and electromagnetic wave tunneling *Appl. Phys. Lett.* **100** 051909

[75] Zhao R, Zhou J, Koschny T, Economou E N and Soukoulis C M 2009 Repulsive Casimir force in chiral metamaterials *Phys. Rev. Lett.* **103** 103602

[76] Zhao R, Zhou J, Koschny T, Economou E N and Soukoulis C M 2010 Comparison of chiral metamaterial designs for repulsive Casimir force *Phys. Rev.* B **81** 235126

[77] Zhao R, Zhou J, Koschny T, Economou E N and Soukoulis C M 2011 Repulsive Casimir forces with finite-thickness slabs *Phys. Rev.* B **83** 075108